NSC95397 is a Novel HIV Latency Reversing Agent

Randilea Nichols Doyle[1+], Vivian Yang[1,2+], Robert Damoiseaux[3,4], Oliver I. Fregoso[1,2]

[1] Department of Microbiology, Immunology, and Molecular Genetics, University of California, Los Angeles, California, USA
[2] Molecular Biology Institute, University of California, Los Angeles, California, USA
[3] California NanoSystems Institute, University of California, Los Angeles, California, USA
[4] Department of Molecular and Medical Pharmacology, University of California, Los Angeles, California, USA

[+] Randilea Nichols Doyle and Vivian Yang contributed equally to this work. Author order was determined alphabetically.

Correspondence: Oliver I. Fregoso
Tel: 310.794.1424
Email: ofregoso@mednet.ucla.edu

Abstract

The latent viral reservoir represents one of the major barriers of curing HIV. Focus on the "kick and kill" approach, in which virus expression is reactivated then cells producing virus are selectively depleted, has led to the discovery of many latency reversing agents (LRAs) that can reactivate latently integrated virus and further our understanding of the mechanisms driving HIV latency and latency reversal. Thus far, individual compounds have yet to be robust enough to work as a therapy, highlighting the importance of identifying new compounds that can act in novel pathways and synergize with known LRAs. In this study, we identified a promising LRA, NSC95397, from a screen of ~4250 compounds in J-Lat cell lines. We validated that NSC95397 reactivates latent viral transcription and protein expression from cells with unique integration events. Cotreating cells with NSC95397 and known LRAs demonstrated that NSC95397 has the potential to synergize with different drugs, such prostratin, a PKC agonist, and SAHA, an HDAC inhibitor. By looking at multiple common markers of open chromatin, we show that NSC95397 does not increase open chromatin globally. Bulk RNA sequencing revealed that NSC95397 does not greatly change cellular transcription. Instead, NSC95397 downregulates many pathways key to metabolism, cell growth, and DNA repair – highlighting the potential of these pathways in regulating HIV latency. Overall, we identified NSC95397 as a novel LRA that does not alter global transcription, that shows potential for synergy with known LRAs, and that may act through novel pathways not previously recognized for their ability to modulate HIV latency.

42 **Introduction**

43 As antiretroviral therapy (ART) has successfully prolonged the life expectancy of HIV positive
44 individuals, these patients are now at higher risk from comorbidities such as cancers and HIV-
45 associated neurocognitive disorders. Latency reversal remains one of the primary hopes of curing
46 HIV infected individuals. However, our lack of understanding about the molecular mechanisms
47 leading to latency and reactivation has impeded our capacity to efficiently reactivate latent HIV.
48 While some components of latency are inherent to the virus, such as the expression of Tat and
49 cis-regulatory elements encoded within HIV, it seems that the primary determinants of latency
50 and reactivation are cellular host factors that control gene expression (1, 2). Once integrated,
51 expression of the HIV provirus is subject to much of the same cellular machinery that regulates
52 host genes. The HIV-1 LTR has multiple binding sites for the transcription factor NF- κB, as well
53 as binding sites for both constitutive (Sp1) and inducible (NF-AT and AP-1) transcription factors
54 (2, 3). Since transcription is dependent on the accessibility of these transcription factor binding
55 sites, histone positioning and epigenetic modifications have large effects on HIV gene expression
56 (1, 2). Consistent with this data, the most promising latency reversing agents (LRAs) attempt to
57 activate host transcription (such as PKC, JNK/MAPK, and NF-κB agonists) and chromatin
58 decondensation (such as histone deacetylase inhibitors, histone methyltransferase inhibitors, and
59 DNA methyltransferase inhibitors). PKC agonists, such as PMA and prostratin, can potently
60 activate latent virus in cell lines but have not been taken to clinical trials for various reasons,
61 including oncogenic potential (4). Similarly, other compounds targeting these pathways, such as
62 Bryostatin-1 and SAHA (Vorinostat), have performed well *in vitro* and *ex vivo* but have had limited
63 success in clinical trials (4, 5). The likely reason for the lack of viable LRAs is the heterogeneity
64 of the viral reservoir *in vivo* (5). To overcome this, new LRAs are needed, especially ones acting
65 through different mechanisms or different pathways. At the same time, mechanistically distinct
66 LRAs have the potential to synergize and increase the desired effect of reactivating latent virus

67 with lower concentrations of drug and thus minimizing side effects. As such, future treatments will
68 likely need to be combinatorial to overcome toxic side effects as well as stimulate as many latent
69 cells as possible.
70
71 To address the need for LRAs stimulating different pathways and mechanisms than current ones,
72 we performed a medium-throughput screen in J-Lat 10.6 cells, a clonally selected Jurkat cell line
73 with an integrated ΔEnv HIV-1 that contains GFP in the place of Nef (6-8). At steady state, these
74 cells express little to no HIV or GFP, but upon activation with a LRA, such as PMA, HIV and GFP
75 are expressed. We started with approximately 4,250 unique small molecules that we narrowed
76 down through multiple steps of validation, including flow cytometry, qPCR, and western blot for
77 both HIV and GFP, to a single compound, NSC95397, which reactivates latent HIV in multiple J-
78 Lat clones with unique integration events. Previously studied for its potential to treat cancer,
79 NSC95397 is a Cdc25 phosphatase inhibitor that can also inhibit many members of the dual-
80 specificity phosphatase (DUSP) family, specifically DUSP1 (MKP1), DUSP6 (MKP3), and
81 DSUP14 (MKP6) (9-12), which are key to cell proliferation and reaction to infection. NSC95397
82 has been primarily studied in cancer cells, with a focus on its ability to inhibit cell growth and
83 induce cell cycle arrest (10). Only a few studies have been conducted in immune cells, where
84 NSC95397 is suggested to be anti-inflammatory through inhibition of serine-threonine kinases
85 such CD45 and SHP-2 (13). Additionally, most transcription factor families associated with HIV
86 transcription are inhibited in NSC95397 treated cells, making the mechanism by which NSC95397
87 activates HIV transcription unclear (14).
88
89 To understand how NSC95397 is activating HIV expression in the J-Lat system, we performed
90 combinatorial studies with current LRAs and found that NSC95397 is not acting upon the same
91 pathways, as it showed a more than additive effect on reactivation when combined with other

92 LRAs. Additionally, analysis of histone marks associated with active transcription indicated that
93 NSC95397 does not alter global histone modifications to reactivate latent HIV. Transcriptome
94 analysis by RNA sequencing found that NSC95397 does not stimulate transcriptional upregulation
95 or Tat-mediated LTR activation. Instead, NSC95397 leads to the downregulation of diverse
96 pathways, including metabolism, cell cycle, hypoxia/redox, and DNA repair. We confirmed that
97 cells treated with NSC95397 have increased accumulation of signaling molecules in the DNA
98 damage repair pathways. Thus, while we were unable to identify an obvious mechanism of action
99 for NSC95397, our data indicates that it acts on different and unknown pathways compared to
100 current LRAs and could be a useful combinatorial therapy in our quest to cure latent HIV-1.
101
102 **Results**
103 NSC95397 is identified as a HIV latency reversal agent (LRA) from a medium-throughput screen.
104 To identify novel compounds and molecular pathways of HIV latency reversal, we conducted a
105 medium-throughput screen of approximately 4,250 compounds (Figure 1A) in J-Lat 10.6 cells, a
106 clonally selected Jurkat cell line with a latently integrated ΔEnv HIV-1 that contains GFP in the
107 place of Nef (6, 7). In the initial screen, we incubated the J-Lat 10.6 cells with individual
108 compounds in 348-well glass-bottom plates for 36 hours, then imaged for GFP expression using
109 an automated ImageExpress microscope (Figure S1 A-B). Using Z-score cutoffs of ≥ 2 for GFP
110 cell count and % of cells GFP positive and ≥ 1 for GFP average intensity, we identified 83
111 compounds for additional testing (Figure 1B-C). Though PMA was a positive control used in this
112 study, we also found it as a hit within the library (light grey square in Figure 1B-C, S1A-B).
113 Additionally, we identified IBET151 (purple diamond), a previously described LRA (15),
114 suggesting our screen is robust enough to identify new potential LRAs (Figure 1B-C, S1A-B). To
115 validate the 83 hits, GFP expression was measured in J-Lat 10.6 cells treated in triplicate and
116 incubated for 24 and 48 hours (Figure 1C). 35 of the 83 compounds validated with repeated GFP

117 expression. Neuronal signaling, DNA damage response (DDR) pathways, and metabolism were
118 the top three pathways targeted by the 35 validated compounds (Figure 1D). Next, we performed
119 EC_{50} titration curves on a subset of the validated compounds in the J-Lat 10.6 and 5A8 cells,
120 another clonal J-Lat line with a unique integration event (8), at 24 and 48 hours (Figure S1C-E).
121 While most compounds further validated at multiple concentrations and with little toxicity, we
122 found that NSC95397 stimulates HIV (GFP) expression in both 10.6 and 5A8 J-Lat cells equal to
123 or more than the LRA positive control PMA (Figure 1E; blue triangle in Figure 1B-C, S1A-B).
124 Unlike NSC95397, which stimulates HIV expression in both J-Lat clonal cell lines, IBET151 only
125 stimulates GFP expression in 10.6 cells (Figure 1F). Through our screen and follow-up validation,
126 we identified NSC95397 as a compound previously not linked to HIV latency reversal that can
127 reactivate HIV expression in multiple latency clones with unique integration events.
128
129 <u>NSC95397 reactivates GFP and p24 expression in J-Lat 10.6 and 5A8 cells.</u>
130 One of the consequences of fluorescence-based screens is the potential for false positives from
131 autofluorescent compounds. To rule out false positives and ensure true HIV reactivation, we
132 assayed hits from our screen for intracellular HIV p24 via flow cytometry, GFP protein expression
133 by flow cytometry and western blot, and HIV-1 and GFP mRNA expression by qRT-PCR. At higher
134 concentrations, NSC95397 is slightly autofluorescent in the GFP channel with 30-40% of cells
135 GFP+ (Figure 2A) vs 20% p24+ (Figure 2B). qPCR confirmed expression of both GFP and
136 unspliced HIV RNA with fold changes ranging 10 – 150 compared to untreated cells (Figure 2 C-
137 D). Lastly, protein expression was confirmed by western blot for GFP in both J-Lat 10.6 and 5A8
138 cells, further indicating that NSC95397-mediated HIV reactivation occurs irrespective of
139 integration site (Figure 2E). In contrast to NSC95397, another hit from the screen was Sunitinib,
140 a receptor tyrosine kinase inhibitor used to treat cancer (Figure S2A). However, no intracellular
141 HIV p24 was detected when measured via flow cytometry (Figure S2B). Consistent with the lack

142 of protein expression, there was no gene expression for GFP or HIV-1 as measured by qRT-PCR
143 (Figure S2D-E). Lastly, autofluorescent ("green") cells were identified in Sunitinib-treated Jurkat
144 cells with flow cytometry (Figure S2C). These data indicate that while Sunitinib is a false positive
145 with autofluorescence in the GFP channel, NSC95397 induces HIV-1 RNA and protein expression
146 in multiple J-Lat clones.
147
148 NSC95397 increases HIV reactivation in combination with established LRAs.
149 While NSC95397 has been studied as a dual-specificity phosphatase inhibitor, it has not been
150 correlated with canonical HIV latency reactivation pathways, nor well-tested in immune cells. To
151 better understand the molecular mechanisms by which NSC95397 reactivates latently integrated
152 HIV-1, we first looked to see whether NSC95397 could synergize with other known latency
153 reversing compounds. We expected that if the combined treatments increase reactivation more
154 than the simple addition of the treatments alone, then the compounds likely act in different,
155 potentially synergistic, pathways.
156
157 We first assessed the potential for NSC95397 to synergize with SAHA, a histone-deacetylase
158 inhibitor. At 1.0 to 12.5 μM, SAHA alone reactivates both J-Lat 10.6 and 5A8 cells in a titratable
159 manner (Figure 3A-B, S3A-B). When combined with 1.5 μM NSC95397 in the J-Lat 10.6 cells,
160 there is a more than additive increase of reactivation, especially with 5.0 μM and 1.0 μM SAHA
161 (Figure 3A, S3A). In the J-Lat 5A8 cells, there is a more than additive increase of reactivation in
162 all combinations (Figure 3B, S3B). There is also a moderate increase in dead GFP+ cells when
163 NSC is combined with SAHA (Figure S3A-B). This suggests that NSC95397 does not act similar
164 to SAHA. To directly determine whether NSC95397 modifies the global epigenetic landscape to
165 increase euchromatin, we treated J-Lat 10.6 and J-Lat 5A8 cells with NSC95397 and assessed
166 the levels of three markers of active promoter and enhancer regions by flow cytometry: H3K4me3,

167 H3K9ac, H3K27ac. In both cell lines, there was little to no change in NSC95397 treated cells
168 compared to untreated cells for all three markers of active chromatin (Figure 3C-D, S4A-D).
169
170 We next assessed the potential for NSC95397 to synergize with prostratin, a PKC agonist that
171 can reactivate latent HIV through NF-κB mediated transcription. In J-Lat 10.6 cells, 0.1 to 0.66
172 μM of prostratin alone lead to a titratable increase of GFP compared to untreated cells (Figure
173 3E, S3C). Similarly, 0.5 to 5.0 μM of prostratin lead to a titratable increase of GFP in J-Lat 5A8
174 cells compared to untreated cells (Figure 3F, S3D). When combined with 1.5 μM NSC95397,
175 there is a more than additive effect for both cell lines (Figure 3E-F, S3C-D), suggesting that
176 prostratin and NSC95397 act in different pathways. Similar to SAHA treated cells, there was also
177 an increase in dead GFP+ cells when NSC and prostratin were combined (Fig S3 C-D). Together,
178 the data suggests that NSC95397 does not directly reactivate latent HIV through NF-κB
179 transcription nor through altering chromatin to allow for active transcription.
180
181 <u>NSC95397 does not increase known HIV-associated transcription pathways.</u>
182 As NSC95397 does not appear to change histone modifications nor act through PKC/NF-κB
183 transcription, we utilized bulk RNA sequencing to identify potential transcriptional pathways
184 associated with NSC95397-mediated latency reversal. J-Lat 10.6 cells were treated with
185 NSC95397 for 24 hours, with PMA and SAHA used as positive controls. PMA and SAHA treated
186 cells group apart in both PCA and cluster analysis, while NSC95397 and group close to the
187 untreated control cells (Figure 4A-B), indicative of their different mechanisms of action. PMA,
188 SAHA, and NSC95397 all increased viral transcripts compared to untreated cells (Figure 4C, S5A,
189 S6). As HIV Tat stimulates LTR transcription and elongation, we also looked for upregulation in
190 Tat-regulated host genes but found little change and correlation to Tat-mediated host transcripts
191 (Figure 4D), suggesting NSC95397 does not specifically work through stimulation of HIV-1 Tat.

192 As some compounds may reactivate latently infected cells due to heat shock stress (16), we also
193 looked for increase in heat shock response transcripts but saw little change in NSC95397 treated
194 cells (Figure 4E). Notably, unlike the positive controls, NSC95397 had very few differentially
195 expressed genes (DEGs) outside of the HIV-1 transcripts, suggesting that NSC95967 may
196 specifically activate the latent HIV and few other genes. Gene Set Enrichment Analysis (GSEA)
197 for enriched hallmarks did not identify any positively enriched hallmarks for NSC95397. This is
198 supported by the lack of increased HIV-related transcription factor transcripts (Figure 4F) as well
199 as the lack of enrichment of transcription factors by TRRUST (transcriptional regulatory
200 relationships unraveled by sentence-based text-mining, http://www.grnpedia.org/trrust) analysis
201 (Figure S5B). While TRRUST also did not show enrichment of transcription-factor-mediated
202 changes for downregulated genes and pathways (Figure S5C), GSEA analysis identified many
203 significant negatively enriched hallmarks, including metabolism, cell cycle, hypoxia/redox, stress
204 response, and DNA damage/repair (Figure 4G, Supplement Table 1). Thus, our RNA sequencing
205 analyses indicate that NSC95397 does not greatly alter the global transcriptional landscape,
206 despite specifically activating HIV transcription.
207
208 <u>NSC95397 increases markers of DNA damage.</u>
209 DNA damage has been linked to transcriptional and epigenomic changes that are related to
210 activating transcriptional pathways, some of which have been correlated with latency reactivation
211 (17, 18). As we identified downregulation of genes in pathways mediating DNA repair by
212 NSC95397 (Figure 4G), we asked if NSC95397 treatment leads to an accumulation of DNA
213 damage. To test this, we treated U2OS cells with DMSO as a negative control, Etoposide, a
214 topoisomerase II inhibitor that induces DNA breaks, as a positive control, PMA, or NSC95397 and
215 probed for three different markers of the DNA damage response (DDR) by immunofluorescence:
216 γH2AX, a general marker of DNA damage, RPA32, a marker of single stranded DNA (ssDNA)

217 lesions, and 53BP1, a marker of double stranded DNA (dsDNA) breaks. NSC95397 treatment led
218 to an increase in γH2AX mean fluorescence intensity when compared to untreated cells, though
219 to a much lesser extent than Etoposide (Figure 5). Similar results were seen for RPA32 and
220 53BP1 when measuring foci per cell; however, the effect on 53BP1 was not as robust as RPA32,
221 suggesting potential specificity in the DDR activation by NSC95397 (Figure 5). Together, this
222 supports our RNA sequencing analysis and suggests that NSC95397 activates the host DDR,
223 particularly ssDNA break pathways.
224

225 **Discussion**

226 In this study, we have identified NSC95397 as a novel LRA that reactivates latent HIV expression
227 differently from previously reported latency reversing mechanisms. Although NSC95397 has been
228 studied as a potential cancer therapeutic, there are few studies in immune cell types and none
229 that explain its ability to reverse HIV latency. NSC95397 broadly inhibits members of the DUSP
230 family and thus change many pathways in cell signaling, therefore it is possible that the compound
231 could dysregulate some of the transcription factor families related to HIV latency reversal and
232 general HIV transcription (2, 3). However, unlike with PMA and SAHA, our RNA sequencing data
233 suggests that NSC95397 does not globally activate transcription pathways associated with HIV
234 latency reversal. This is true even with the shared downregulation of Myc and Myc-associated
235 pathways, which has been shown to promote proviral latency (19). In fact, at the concentration
236 and timing we used, there are very little differentially expressed genes and the overall
237 transcriptome remains very similar to untreated cells. This, along with the lack of change in global
238 histone markers we checked, suggests that NSC95397 may cause little side effects and make it
239 an ideal drug to consider for cure therapy.
240

241 At the same time, the lack of global changes epigenetically and transcriptionally suggests the
242 possibility that NSC95397 reactivates latent HIV through mechanisms that are either LTR specific
243 or not yet tied to latency modulation. Since NSC95397 is a broad dual-specificity phosphatase
244 inhibitor, further exploring changes in global proteomics, phosphoproteomics, and post-
245 translational modifications to identify protein networks affected would help to understand how
246 latency can be governed and may elucidate new pathways involved in HIV latency and
247 reactivation. Similarly, since RNA sequencing showed shutdown of metabolism, DNA repair,
248 hypoxia/stress response, and generally anabolic pathways in addition to Myc-associated
249 pathways, it would be important to look at how changes in metabolism and the metabolic
250 microenvironment can influence latency.
251
252 Of the enriched downregulated pathways, the shutdown of DNA repair especially stood out to us
253 due to data implicating the DNA damage response (DDR) in HIV replication. Early studies with
254 UV have shown that DNA damage can increase HIV transcription (20, 21). Similarly, members of
255 the DDR have been tangentially implicated in mechanisms related to latency modulation (18, 22).
256 This opens the potential for NSC95397 to reactivate latent viral transcription through the
257 downstream effects of turning off portions of the DDR and the accumulation of DNA damage
258 markers as well as increasing the effects of DNA-damage-related transcription from expressed
259 viral proteins. At the same time, there is an increase in the reactivation profile of dead cells treated
260 with NSC95397, which could suggest a sensitivity to DNA damage post reactivation. Our data
261 highlights that further specific studies need to be done to define the precise connections between
262 the DDR and latency reactivation, both generally and with NSC95397.
263
264 Despite its currently unknown mechanisms of action for HIV latency reversal, the potential for
265 NSC95397 to synergize with other compounds is an important consideration for future work, since

266 single LRAs have not performed well on their own in clinical trials. Additionally, combining
267 synergistic LRAs allows for lower concentrations of each compound, thus maximizing efficiency
268 while lowering toxicity and other side effects. We showed that NSC95397 not only has a greater
269 than additive effect when combined with either prostratin or SAHA, but also increases the
270 proportion of reactivated cells in the dead population, as mentioned above. This demonstrates a
271 potential for NSC95397 or future derivatives to work well with other LRAs for activating cells with
272 latent HIV, while also sensitizing reactivated cells to death through DNA damage or other
273 mechanisms. Interestingly, the two J-Lat clonal cell lines we used responded, both in HIV
274 expression and cell toxicity, to NSC95397 co-treatments differentially, suggesting that there may
275 be integration site specific responses (Figure S3). While this could be explained by cell line
276 specific properties, it highlights the issue with reservoir heterogeneity and the importance of
277 formulating LRA cocktails that target multiple pathways and will reach a greater proportion of the
278 latent viral reservoir.
279
280 Another key consideration is as the population of HIV infected individuals is getting older, there
281 has been an increase in AIDS and non-AIDS related cancers (23-25), with cancer as one of the
282 leading causes of death for HIV positive individuals on ART (23-25). However, the effect of
283 chemotherapy on the expansion or contraction of the latent HIV reservoir has not been explored,
284 highlighting the importance in understanding how the drug regimens interact to affect HIV
285 infection, latency, and cancers. While NSC95397 is not currently used to treat cancer, given the
286 importance of Cdc25 inhibition in cancer therapy, NSC95397 represents an interesting compound
287 to further test in the scope of HIV infected individuals who develop cancer. Moreover, our study
288 sets the foundation to test additional cancer therapies for their impact on HIV replication and the
289 latent viral reservoir.
290

291 In summary, our results present NSC95397, a novel LRA with an unknown mechanism that
292 exhibits important characteristics as an LRA: potential for synergizing with known LRAs and little
293 change in global transcription and chromatin landscape. In future studies, to better understand
294 latency modulation and find a new direction for LRA development, it will be important to follow up
295 on the specific mechanism by which NSC95367 reactivates latent HIV, how it specifically affects
296 immune cells both infected and not, and how well the compound performs as an LRA *in vivo*.
297

298 **Acknowledgements**

299 We would like to thank the UCLA Molecular Screening Shared Resource, especially Bobby Tofig
300 and Constance Yuen, for their help with performing the drug screen and analysis. Flow cytometry
301 was performed in the UCLA Jonsson Comprehensive Cancer Center (JCCC) and Center for AIDS
302 Research Flow Cytometry Core Facility. We thank the UCLA Technology Center for Genomics &
303 Bioinformatics for performing the RNA sequencing library preparation and sequencing. We would
304 also like to thank Jeff Long and Steve Jacobsen (UCLA) for the use of the LSM 980. We thank
305 Warner Greene for generously sending us the J-Lat 5A8 cells used in this study. This research
306 was funded by NIH NIAID grant R01AI147837 (O.I.F.) and a UCLA DGSOM I3T Discovery Seed
307 Grant (O.I.F), with support from the Ruth L. Kirschstein National Research Service Award
308 AI007323 (R.N.D, V.Y.). The funders had no role in study design, data collection and
309 interpretation, or the decision to submit the work for publication.
310

311 **Author Contributions**

312 Experimental Concept and Design: R.N.D., V.Y., R.D., O.I.F.
313 Experiment Execution: R.N.D., V. Y.
314 Manuscript Writing and Editing: R.N.D., V.Y., O.I.F.
315

316 **Materials and Methods**

317 **Cell Lines and Culture**

318 The J-Lat 10.6 and 5A8 cells were cultured in flasks (Thermo Fisher Nunc™ EasYFlask™) in
319 RPMI 1640 growth medium (L-glutamine, Gibco) with 10% fetal bovine serum (Gibco) and 1%
320 penicillin-streptomycin (Gibco) and the human bone osteosarcoma epithelial (U2OS) cells were
321 cultured as adherent cells directly on tissue culture plastic (Greiner) in DMEM growth medium
322 (high glucose, L-glutamine, no sodium pyruvate; Gibco) with 10% fetal bovine serum (Gibco) and
323 1% penicillin-streptomycin (Gibco) at 37°C and 5% CO2. U2OS cells were harvested using 0.05%
324 Trypsin-EDTA (Gibco).

325

326 **Medium-throughput compound screen**

327 J-Lat 10.6 or 5A8 cells were seeded into 384-well black, glass-bottom plates (Greiner) using an
328 Agilent BioTek Multiflo. All compounds were stored at 10 mM in DMSO, and 0.25 µl was added
329 to each well using a Biomek Fx (Beckman Coulter). Media containing 0.25 µl DMSO or 5.0 ng/mL
330 PMA was added to the first and last two columns, respectively. Cells were incubated for 24, 36,
331 or 48 hours. Cells incubated with Hoechst (Invitrogen H3570) for 15 minutes then each plate was
332 imaged using ImageXpress Micro Confocal High Content Imaging System (Molecular Devices).
333 Images were analyzed using the MetaXpress Analysis software, and the raw data was imported
334 into the Collaborative Drug Discovery vault online to generate Z scores. The EC_{50} was conducted
335 similarly; each compound was purchased new, resuspended at 10 mM in DMSO, then a 10-step
336 4-fold dilution was pipetted down the plate. Follow up studies were done manually with IBET151
337 (Cayman Chemistry 11181), NSC95397 (Cayman Chemistry 21431), PMA (VWR 102515-692),
338 prostratin (Cayman Chemistry 10272), SAHA (Cayman Chemistry 10009929), and Sunitinib
339 (Cayman Chemistry 13159).

340

341 **Flow cytometry**

342 J-Lat 10.6 or 5A8 cells were plated in U-bottom 96-well microplates (Corning Inc) at $1x10^6$
343 cells/mL in plain or drug media for 24 hours. Cells were then incubated with Ghost Dye (Ghost
344 Dye™ Red 780) (1:4000 µL PBS) for 30 min at 4°C, then fixed with 4% PFA for 15 min.
345 Alternatively, cells were fixed with 4% PFA for 10 min, then permeabilized with 0.1% Saponin for
346 5 minutes and probed with anti-H3K4me3 (Cell Signaling 12064S, 1:150 in 0.1% Saponin), anti-
347 H3K9ac (Cell Signaling C5B11, 1:150 in 0.1% Saponin), anti-H3K27ac (Cell Signaling D5E4,
348 1:150 in 0.1% Saponin), or anti-p24 (Beckman Coulter 6604667, 1:250 in 0.1% Saponin) for 1
349 hour, in the dark as necessary. Cells were analyzed with an Attune NxT Flow Cytometer (Thermo
350 Fisher Scientific) and data analysis was performed with FlowJo (BD).

351

352 **Western Blots**

353 J-Lat 10.6 or 5A8 cells were plated in 6-well tissue culture-treated plates (Greiner Bio-one) at
354 ($5x10^6$ cells/mL) in plain or drug media for 24 hrs. Cells were then lysed in
355 radioimmunoprecipitation assay (RIPA) buffer (150 mM NaCl, 1% NP-40, 0.5% DOC, 0.1% SDS,
356 50 mM Tris) for 15 min on ice and clarified by centrifugation at 14,800 x g for 15 minutes. Lysates
357 were boiled in 4x sample buffer (250 mM Tris-HCL, 8% SDS, 0.2% Bromophenol Blue, 40%
358 Glycerol, 20% β-mercaptoethanol) in preparation for SDS-PAGE using 12% Bis-Tris
359 polyacrylamide gels (Invitrogen) and transferred to polyvinylidene difluoride membranes.
360 Immunoblotting was performed using mouse anti-eGFP (Takara, 1:2000), rabbit anti-Actin
361 (Bethyl, 1:6000), mouse anti-gag (NIH-ARP#3537, 1:1000) followed by donkey anti-rabbit IgG
362 800CW (IRDye®,1:20000) or donkey anti-mouse IgG 680RD (IRDye®,1:20000) and imaged on
363 a LI-COR Odyssey M.

364

365 **RNA Isolation**

366 Total RNA was isolated from $4x10^6$ J-Lat 10.6 cells according to the W.M. Keck Foundation
367 Biotechnology Resource Laboratory at Yale University TRIzol RNA Isolation protocol (26).
368
369 **qRT-PCR**
370 250 ng of input RNA was used as template for reverse transcription by SuperScript IV First-Stand
371 Synthesis System (Invitrogen) with Oligo(dT) primers. qRT-PCR was performed with PowerTrack
372 SYBR Green Master Mix (Thermo Fisher Scientific) on the LightCycler 480 System (Roche) with
373 the following primers: (5' to 3') HIV-1 unspliced RNA GCGACGAAGACCTCCTCAG and
374 GAGGTGGGTTGCTTTGATAGAGA and GAPDH
375 CAAGATCATCAGCAATGCCT and AGGGATGATGTTCTGGAGAG. Initial enzyme activation at
376 95°C for 2 minutes, then 40 cycles of 95°C for 15 seconds and 60°C for 60 seconds. mRNA levels
377 were quantified by calculating ΔΔCt. Target transcript Ct values were normalized to the Ct value
378 of the housekeeping gene GAPDH followed by calculating fold change to untreated cells.
379
380 **RNA Library Prep and Sequencing**
381 Libraries for RNA-Seq were prepared with KAPA Stranded mRNA-Seq Kit (Cat.KK8420). The
382 workflow consists of mRNA enrichment and fragmentation, first strand cDNA synthesis using
383 random priming followed by second strand synthesis converting cDNA:RNA hybrid to double-
384 stranded cDNA (dscDNA), and incorporates dUTP into the second cDNA strand. cDNA
385 generation is followed by end repair to generate blunt ends, A-tailing, adaptor ligation and PCR
386 amplification. Different adaptors were used for multiplexing samples in one lane. Sequencing was
387 performed on Illumina NovaSeq 6000 for PE 2x50 run. Data quality check was done on Illumina
388 SAV. Demultiplexing was performed with Illumina Bcl2fastq v2.19.1.403 software.
389
390 **RNA Sequencing Analysis**

391 Fastq files were run through FastQC and MultiQC to check the quality of raw sequence data (27,
392 28). A custom reference genome was generated by combining the Genome Reference
393 Consortium Human build 38 (GRCh38/hg38) and the HIV-1 genome specific to J-Lat 10.6 (6)
394 before aligning the reads to the genome through STAR (29). Aligned reads were then normalized
395 through the DESeq2 package in R (30). R package EnhancedVolcano was used to visualize
396 specific gene subsets (31). Gene lists were sorted and filtered for log2FoldChange above 2.
397 Upregulated and downregulated gene lists were submitted to Metascape [https://metascape.org]
398 for drug specific and cross comparison analyses (32). Top 500 up/downregulated genes were
399 taken for drug specific Metascape analysis. Top 1000 up/downregulated genes were taken for
400 drug cross comparison Metascape analysis. Gene set enrichment analysis (GSEA) was
401 performed to identify the statistically significant hallmark gene sets from each drug treatment
402 compared to untreated cells (33, 34).
403
404 **Immunofluorescence Microscopy**
405 U2OS cells were plated on glass coverslips in 6-well tissue culture-treated plates (Greiner Bio-
406 one) overnight and then switched into plain or drugged media consisting of either 5.0 ng/mL PMA,
407 50.0 µM Etoposide, 5.0 µM NSC95397, or 10.0 µL DMSO for 24 hours. Cells were then fixed in
408 4% PFA for 15 minutes and permeabilized with 1% Triton-X 100 in PBS for 5-10 min at 4°C. Cells
409 were then blocked with immunofluorescence (IF) block buffer (3% BSA in PBS) for 1 hour and
410 incubated with primary antibodies: rabbit anti-γH2A.x (Cell Signaling 9718, 1:2000), rabbit anti-
411 RPA32 (GeneTex GTX113004 1:2000), or rabbit anti-53BP1 (Cell Signaling S1778, 1:2000)
412 overnight at 4°C. Coverslips were washed three times with PBS then incubated with secondary
413 antibodies (Alexa Fluor 488 or 594) and Hoechst 33342 (1:2000) for 1 hour. Coverslips were then
414 washed three times with PBS and mounted onto slides with ProLong™ Gold Antifade Mountant
415 (Invitrogen) and sealed when dried. Images were obtained with a ZEISS LSM 980.

416 **Figure Legends**

417 **Figure 1. NSC95397 identified as a HIV latency reversal agent (LRA) from a medium-**
418 **throughput screen. A)** Schematic detailing the screen methodology. **B-C)** Z-scores of total cell
419 count or GFP intensity vs percent of cells GFP positive. The grey square and purple diamond are
420 two known latency reversal agents, PMA and IBET151, respectively, and the blue triangle is a
421 previously unknown LRA, NSC95397. **D)** 83 compounds were rescreened in triplicate at 24 and
422 48 hours. Each row of the heatmap represents a different compound, with the top and second
423 row being the controls: untreated (UT) and PMA. **E)** A circle graph representing the
424 pathways/targets of the 35 compounds that revalidated in **D**. **F-G)** The EC_{50} titration of NSC95397
425 and IBET151 in J-Lat 10.6 and 5A8 cells. PMA was used as a positive control at 50nM.

426

427 **Supplemental Figure 1. NSC95397 and IBET151 were identified as HIV LRAs of interest**
428 **from a medium-throughput screen. A-B)** The raw screen data of total cell count or GFP
429 intensity vs percent of cells GFP positive. The grey square and purple diamond are two known
430 latency reversal agents, PMA and IBET151, respectively, and the blue triangle is a previously
431 unknown LRA, NSC95397. **C)** Example plate map of the EC_{50} screen. Each compound was
432 screened in triplicate and across the plate is a 4-fold concentration decrease. The first two
433 columns and last row were treated with the vehicle control, DMSO, and the last two columns were
434 treated with the positive control, PMA. **D-E)** The percent of GFP positive cells, top green plate,
435 and dead PI positive cell, lower red plate, measured during our EC_{50} titration experiment in J-Lat
436 10.6 (**D**) and 5A8 cells (**E**). Related to Figure 1.

437

438 **Figure 2. NSC reactivates GFP and p24 expression in J-Lat 10.6 and 5A8 cells.** J-Lat 10.6
439 (**A-E**) or 5A8 (**F**) cells were untreated or treated with 5.0 ng/mL PMA (positive control), or a titration
440 of NSC95397 (NSC) from 12.5 µM to 1.0 µM. **A-B)** Bar graphs showing GFP expression (**A**) or

441 intracellular HIV p24 (**B**) measured via flow cytometry. **C-D)** Bar graphs showing GFP (**C**) or
442 unspliced HIV RNA transcripts (**D**) measured via qRT-PCR. **E-F)** Western blot of whole cell
443 lysates of either J-Lat 10.6 (**E**) or 5A8 cells (**F**) probed for GFP and actin (loading control). 25.0
444 µM SAHA was used as appositive control. L = ladder; UT = untreated. Results were analyzed
445 with a one-way ANOVA with Dunnett multiple comparisons tests in **A-B** or an unpaired t test in
446 **C-D**; ns = not significant, * = $p \leq 0.0332$, ** = $p \leq 0.0021$, *** = $p \leq 0.0002$, **** = $p \leq 0.0001$.
447
448 **Supplemental Figure 2. Sunitinib is one of a subset of false positives identified in a J-Lat**
449 **screen for LRAs.** J-Lat 10.6 or parental Jurkat cells were untreated or treated with 5.0 ng/mL
450 PMA (positive control), or a titration of Sunitinib (SU) from 5.0 – 1.0 µM. **A-B)** Bar graphs showing
451 GFP (**A**) or intracellular HIV p24 (**B**) measured via flow cytometry in J-Lat 10.6 cells. **C)** A bar
452 graph of GFP measured via flow cytometry in treated Jurkat cells. **D-E)** Bar graphs showing GFP
453 (**D**) or unspliced HIV RNA transcripts (**E**) measured via qRT-PCR. Related to Figure 2.
454
455 **Figure 3. NSC95397 increases HIV reactivation in combination with established LRAs. A-**
456 **B)** J-Lat 10.6 (**A**) or 5A8 (**B**) cells were untreated or treated with 5.0 ng/mL PMA (positive control),
457 NSC95397 (NSC) at 1.5 µM, a titration of SAHA from 12.5 – 1.0 µM, or a titration of SAHA with
458 NSC held constant at 1.5µM. Bar graphs show GFP mean fluorescence intensity (MFI) measured
459 via flow cytometry. **C-D)** J-Lat 10.6 (**C**) or 5A8 (**D**) cells were untreated or treated with 5.0 ng/mL
460 PMA, 25.0 µM SAHA (positive control), or NSC at 2.5 µM. Bar graphs show H3K9ac MFI
461 measured by flow cytometry. **E-F)** J-Lat 10.6 (**E**) or 5A8 (**F**) cells were untreated or treated with
462 5.0 ng/mL PMA, NSC at 1.5µM, a titration of prostratin (PS) from 0.66 – 0.1 µM (**E**) or 5 – 0.5 µM
463 (**F**), or a titration of PS with NSC held constant at 1.5 µM. Bar graphs show GFP MFI measured
464 via flow cytometry. Results were analyzed with a one-way ANOVA with Dunnett multiple

465 comparisons tests; ns = not significant, * = $p \leq 0.0332$, ** = $p \leq 0.0021$, *** = $p \leq 0.0002$, **** =
466 $p \leq 0.0001$.
467
468 **Supplemental Figure 3. NSC95397 increases HIV reactivation and cytotoxicity in**
469 **combination with established LRAs.** Stacked graphs show percent of cells from the full
470 population that are either dead (ghost dye positive) and GFP- (black), dead and GFP+ (blue), live
471 and GFP+ (green), or live and GFP- (white) stacked to a total of 100%. **A-B)** J-Lat 10.6 (**A**) or
472 5A8 (**B**) cells were untreated or treated with 5.0 ng/mL PMA (positive control), NSC95397 (NSC)
473 at 1.5 µM, a titration of SAHA from 12.5 – 1.0 µM, or a titration of SAHA with NSC held constant
474 at 1.5 µM. **C-D)** J-Lat 10.6 (**C**) or 5A8 (**D**) cells were untreated or treated with 5.0 ng/mL PMA,
475 NSC at 1.5 µM, a titration of prostratin (PS) from 0.66 – 0.1 µM (**C**) or 5.0 – 0.5 µM (**D**), or a
476 titration of PS with NSC held constant at 1.5 µM. Related to Figure 3 and Supplemental Figure 4.
477
478 **Supplemental Figure 4. NSC95397 does not change global histone modifications for open**
479 **chromatin.** J-Lat 10.6 (**A, C**) or 5A8 (**B, E**) cells were untreated or treated with 5.0 ng/mL PMA,
480 25.0 µM SAHA (positive control for histone modifications), or 2.5 µM NSC. Bar graphs show
481 H3K4me3 (**A-B**) or H3K27ac (**C-D**) MFI measured by flow cytometry. Results were analyzed with
482 a one-way ANOVA with Dunnett multiple comparisons tests; ns = not significant, * = $p \leq 0.0332$,
483 ** = $p \leq 0.0021$, *** = $p \leq 0.0002$, **** = $p \leq 0.0001$. Related to Figure 3 and Supplemental Figure
484 3.
485
486 **Figure 4. NSC95397 does not globally activate HIV latency reversal associated pathways.**
487 J-Lat 10.6 cells were untreated or treated with 5.0 ng/mL PMA, 25.0 µM SAHA, or 5.0 µM SAHA
488 NSC95397 (NSC) and analyzed by bulk RNA sequencing in four biological replicates. **A)** Principal
489 component analysis (PCA) of all normalized transcripts in all samples. **B)** Clustered heatmap of

490 all normalized transcripts in all samples. **C-F)** Volcano plot labeling HIV-associated reads (**C**),
491 selected HIV Tat-modulated genes (**D**), key heat shock response genes (**E**), and HIV-associated
492 transcription factors (**F**). Cut-offs are drawn for log2 fold change above 1 and p-value greater than
493 0.05 where reads are separated to non-significant and non-enriched (gray), non-significant with
494 log2 fold change above 1.0 (green), significant and log2 fold change below 1.0 (blue), or
495 significant and log2 fold change above 1.0 (red). **G)** Gene ontology using Gene Set Enrichment
496 Analysis (GSEA) identifying top negatively enriched hallmarks.
497
498 **Supplemental Figure 5. NSC95397 has a minimal effect on global transcription.** J-Lat 10.6
499 cells were untreated or treated with 5.0 ng/mL PMA, 25.0 µM SAHA, or 5.0 µM NSC95397 (NSC)
500 and used for bulk RNA sequencing in four biological replicates. **A)** Bar graph showing log2 fold
501 change of HIV associated reads normalizing cells treated with PMA (grey), SAHA (orange), or
502 NSC95397 (blue) against untreated cells. **B-C)** Gene ontology using Metascape for TRRUST
503 analysis of upregulated (left) and downregulated (right) genes for all three treatments (**B**) and
504 NSC95397 alone (**C**). Related to Figure 4 and Supplemental Figure 6.
505
506 **Supplemental Figure 6. PMA and SAHA change latency modulating pathways.** J-Lat 10.6
507 cells were untreated or treated with 5.0 ng/mL PMA or 25.0 µM SAHA and used for bulk RNA
508 sequencing in four biological replicates. **A-B)** Volcano plot highlighting HIV-associated reads in
509 cells treated with PMA (**A**) or SAHA (**B**). **C-D)** Volcano plots highlighting HIV-associated
510 transcription factors in cells treated with PMA (**C**) or SAHA (**D**). **E-F)** Volcano plots highlighting
511 selected HIV Tat-modulated genes in cells treated with PMA (**E**) or SAHA (**F**). **G-H)** Volcano plots
512 highlighting key heat shock response genes in cells treated with PMA (**G**) or SAHA (**H**). Cut-offs
513 are drawn for log2 fold change above 1 and p-value greater than 0.05 where reads are separated
514 to non-significant and non-enriched (gray), non-significant with log2 fold change above 1.0

515 (green), significant and log2 fold change below 1.0 (blue), or significant and log2 fold change
516 above 1.0 (red). Related to Figure 3 and Supplemental Figure 5.
517
518 **Figure 5. NSC95397 causes accumulation of DNA damage markers. A)** Representative
519 images of U2OS cells untreated or treated with 10.0 µL DMSO (negative control), 50.0 µM
520 Etoposide (ETOP; DNA damage positive control), 5.0 ng/mL PMA, or 5.0 µM NSC95397 (NSC)
521 for 24 hours and assessed for presence of DNA damage markers by confocal microscopy. Blue
522 (Hoechst 33342) shows nuclei while damage markers (γH2AX, RPA32, or p53BP1) are in red. **B)**
523 Mean fluorescence intensity (MFI) of at least 100 cells per condition was quantified for γH2AX.
524 Foci per cell of at least 100 cells per condition was quantified for RPA32 and 53BP1 where foci
525 above the ETOP control are binned at 60 (RPA32) or 15 (53BP1). Results were analyzed with a
526 one-way ANOVA with Dunnett multiple comparisons tests; ns = not significant, * = $p \leq 0.0332$, **
527 = $p \leq 0.0021$, *** = $p \leq 0.0002$, **** = $p \leq 0.0001$.

528 **References**

529 1. Mbonye U, Karn J. 2017. The Molecular Basis for Human Immunodeficiency Virus
530 Latency. Annu Rev Virol 4:261-285.
531 2. Siliciano RF, Greene WC. 2011. HIV latency. Cold Spring Harb Perspect Med
532 1:a007096.
533 3. Roebuck KA, Saifuddin M. 1999. Regulation of HIV-1 transcription. Gene Expr 8:67-84.
534 4. Spivak AM, Planelles V. 2018. Novel Latency Reversal Agents for HIV-1 Cure. Annu
535 Rev Med 69:421-436.
536 5. Ait-Ammar A, Kula A, Darcis G, Verdikt R, De Wit S, Gautier V, Mallon PWG, Marcello
537 A, Rohr O, Van Lint C. 2019. Current Status of Latency Reversing Agents Facing the
538 Heterogeneity of HIV-1 Cellular and Tissue Reservoirs. Front Microbiol 10:3060.
539 6. Chung CH, Mele AR, Allen AG, Costello R, Dampier W, Nonnemacher MR, Wigdahl B.
540 2020. Integrated Human Immunodeficiency Virus Type 1 Sequence in J-Lat 10.6.
541 Microbiol Resour Announc 9.
542 7. Jordan A, Bisgrove D, Verdin E. 2003. HIV reproducibly establishes a latent infection
543 after acute infection of T cells in vitro. EMBO J 22:1868-77.
544 8. Chan JK, Bhattacharyya D, Lassen KG, Ruelas D, Greene WC. 2013.
545 Calcium/calcineurin synergizes with prostratin to promote NF-kappaB dependent
546 activation of latent HIV. PLoS One 8:e77749.
547 9. Peyregne VP, Kar S, Ham SW, Wang M, Wang Z, Carr BI. 2005. Novel hydroxyl
548 naphthoquinones with potent Cdc25 antagonizing and growth inhibitory properties. Mol
549 Cancer Ther 4:595-602.
550 10. Dubey NK, Peng BY, Lin CM, Wang PD, Wang JR, Chan CH, Wei HJ, Deng WP. 2018.
551 NSC 95397 Suppresses Proliferation and Induces Apoptosis in Colon Cancer Cells
552 through MKP-1 and the ERK1/2 Pathway. Int J Mol Sci 19.
553 11. Marti F, Krause A, Post NH, Lyddane C, Dupont B, Sadelain M, King PD. 2001.
554 Negative-feedback regulation of CD28 costimulation by a novel mitogen-activated
555 protein kinase phosphatase, MKP6. J Immunol 166:197-206.
556 12. Seo H-Y, Cho S-Y. 2011. *In vivo* Effect of NSC-95397 as a DUSP14 Inhibitor. Bulletin of
557 the Korean Chemical Society 32:4438-4440.
558 13. Stanford SM, Panchal RG, Walker LM, Wu DJ, Falk MD, Mitra S, Damle SS, Ruble D,
559 Kaltcheva T, Zhang S, Zhang ZY, Bavari S, Barrios AM, Bottini N. 2012. High-throughput

560 screen using a single-cell tyrosine phosphatase assay reveals biologically active
561 inhibitors of tyrosine phosphatase CD45. Proc Natl Acad Sci U S A 109:13972-7.
562 14. Yang Y, Yang WS, Yu T, Yi YS, Park JG, Jeong D, Kim JH, Oh JS, Yoon K, Kim JH,
563 Cho JY. 2014. Novel anti-inflammatory function of NSC95397 by the suppression of
564 multiple kinases. Biochem Pharmacol 88:201-15.
565 15. Boehm D, Calvanese V, Dar RD, Xing S, Schroeder S, Martins L, Aull K, Li PC,
566 Planelles V, Bradner JE, Zhou MM, Siliciano RF, Weinberger L, Verdin E, Ott M. 2013.
567 BET bromodomain-targeting compounds reactivate HIV from latency via a Tat-
568 independent mechanism. Cell Cycle 12:452-62.
569 16. Timmons A, Fray E, Kumar M, Wu F, Dai W, Bullen CK, Kim P, Hetzel C, Yang C, Beg
570 S, Lai J, Pomerantz JL, Yukl SA, Siliciano JD, Siliciano RF. 2020. HSF1 inhibition
571 attenuates HIV-1 latency reversal mediated by several candidate LRAs In Vitro and Ex
572 Vivo. Proc Natl Acad Sci U S A 117:15763-15771.
573 17. Christmann M, Kaina B. 2013. Transcriptional regulation of human DNA repair genes
574 following genotoxic stress: trigger mechanisms, inducible responses and genotoxic
575 adaptation. Nucleic Acids Res 41:8403-20.
576 18. White CH, Moesker B, Beliakova-Bethell N, Martins LJ, Spina CA, Margolis DM,
577 Richman DD, Planelles V, Bosque A, Woelk CH. 2016. Transcriptomic Analysis
578 Implicates the p53 Signaling Pathway in the Establishment of HIV-1 Latency in Central
579 Memory CD4 T Cells in an In Vitro Model. PLoS Pathog 12:e1006026.
580 19. Jiang G, Espeseth A, Hazuda DJ, Margolis DM. 2007. c-Myc and Sp1 contribute to
581 proviral latency by recruiting histone deacetylase 1 to the human immunodeficiency virus
582 type 1 promoter. J Virol 81:10914-23.
583 20. Stanley SK, Folks TM, Fauci AS. 1989. Induction of expression of human
584 immunodeficiency virus in a chronically infected promonocytic cell line by ultraviolet
585 irradiation. AIDS Res Hum Retroviruses 5:375-84.
586 21. Miller SC, Taylor A, Watanabe K, Mok K, Torti FM. 1997. Regulation of NF-kappaB and
587 HIV-1 LTR activity in mouse L cells by ultraviolet radiation: LTR trans-activation in a
588 nonirradiated genome in heterokaryons. Exp Cell Res 230:9-21.
589 22. Besnard E, Hakre S, Kampmann M, Lim HW, Hosmane NN, Martin A, Bassik MC,
590 Verschueren E, Battivelli E, Chan J, Svensson JP, Gramatica A, Conrad RJ, Ott M,
591 Greene WC, Krogan NJ, Siliciano RF, Weissman JS, Verdin E. 2016. The mTOR
592 Complex Controls HIV Latency. Cell Host Microbe 20:785-797.

593 23. Albini L, Calabresi A, Gotti D, Ferraresi A, Festa A, Donato F, Magoni M, Castelli F,
594 Quiros-Roldan E. 2013. Burden of non-AIDS-defining and non-virus-related cancers
595 among HIV-infected patients in the combined antiretroviral therapy era. AIDS Res Hum
596 Retroviruses 29:1097-104.
597 24. Herida M, Mary-Krause M, Kaphan R, Cadranel J, Poizot-Martin I, Rabaud C, Plaisance
598 N, Tissot-Dupont H, Boue F, Lang JM, Costagliola D. 2003. Incidence of non-AIDS-
599 defining cancers before and during the highly active antiretroviral therapy era in a cohort
600 of human immunodeficiency virus-infected patients. J Clin Oncol 21:3447-53.
601 25. Yanik EL, Napravnik S, Cole SR, Achenbach CJ, Gopal S, Olshan A, Dittmer DP,
602 Kitahata MM, Mugavero MJ, Saag M, Moore RD, Mayer K, Mathews WC, Hunt PW,
603 Rodriguez B, Eron JJ. 2013. Incidence and timing of cancer in HIV-infected individuals
604 following initiation of combination antiretroviral therapy. Clin Infect Dis 57:756-64.
605 26. Chomczynski P, Mackey K. 1995. Short technical reports. Modification of the TRI
606 reagent procedure for isolation of RNA from polysaccharide- and proteoglycan-rich
607 sources. Biotechniques 19:942-5.
608 27. Ewels P, Magnusson M, Lundin S, Kaller M. 2016. MultiQC: summarize analysis results
609 for multiple tools and samples in a single report. Bioinformatics 32:3047-8.
610 28. Andrews S. 2010. FastQC: a quality control tool for high throughput sequence data.,
611 Babraham Bioinformatics, http://www.bioinformatics.babraham.ac.uk/projects/fastqc
612 29. Dobin A, Davis CA, Schlesinger F, Drenkow J, Zaleski C, Jha S, Batut P, Chaisson M,
613 Gingeras TR. 2013. STAR: ultrafast universal RNA-seq aligner. Bioinformatics 29:15-21.
614 30. Love MI, Huber W, Anders S. 2014. Moderated estimation of fold change and dispersion
615 for RNA-seq data with DESeq2. Genome Biol 15:550.
616 31. Blighe K, S Rana, and M Lewis. 2018. EnhancedVolcano: Publication-ready volcano
617 plots with enhanced colouring and labeling,
618 https://github.com/kevinblighe/EnhancedVolcano.
619 32. Zhou Y, Zhou B, Pache L, Chang M, Khodabakhshi AH, Tanaseichuk O, Benner C,
620 Chanda SK. 2019. Metascape provides a biologist-oriented resource for the analysis of
621 systems-level datasets. Nat Commun 10:1523.
622 33. Subramanian A, Tamayo P, Mootha VK, Mukherjee S, Ebert BL, Gillette MA, Paulovich
623 A, Pomeroy SL, Golub TR, Lander ES, Mesirov JP. 2005. Gene set enrichment analysis:
624 a knowledge-based approach for interpreting genome-wide expression profiles. Proc
625 Natl Acad Sci U S A 102:15545-50.

626 34. Liberzon A, Birger C, Thorvaldsdottir H, Ghandi M, Mesirov JP, Tamayo P. 2015. The
627 Molecular Signatures Database (MSigDB) hallmark gene set collection. Cell Syst 1:417-
628 425.
629

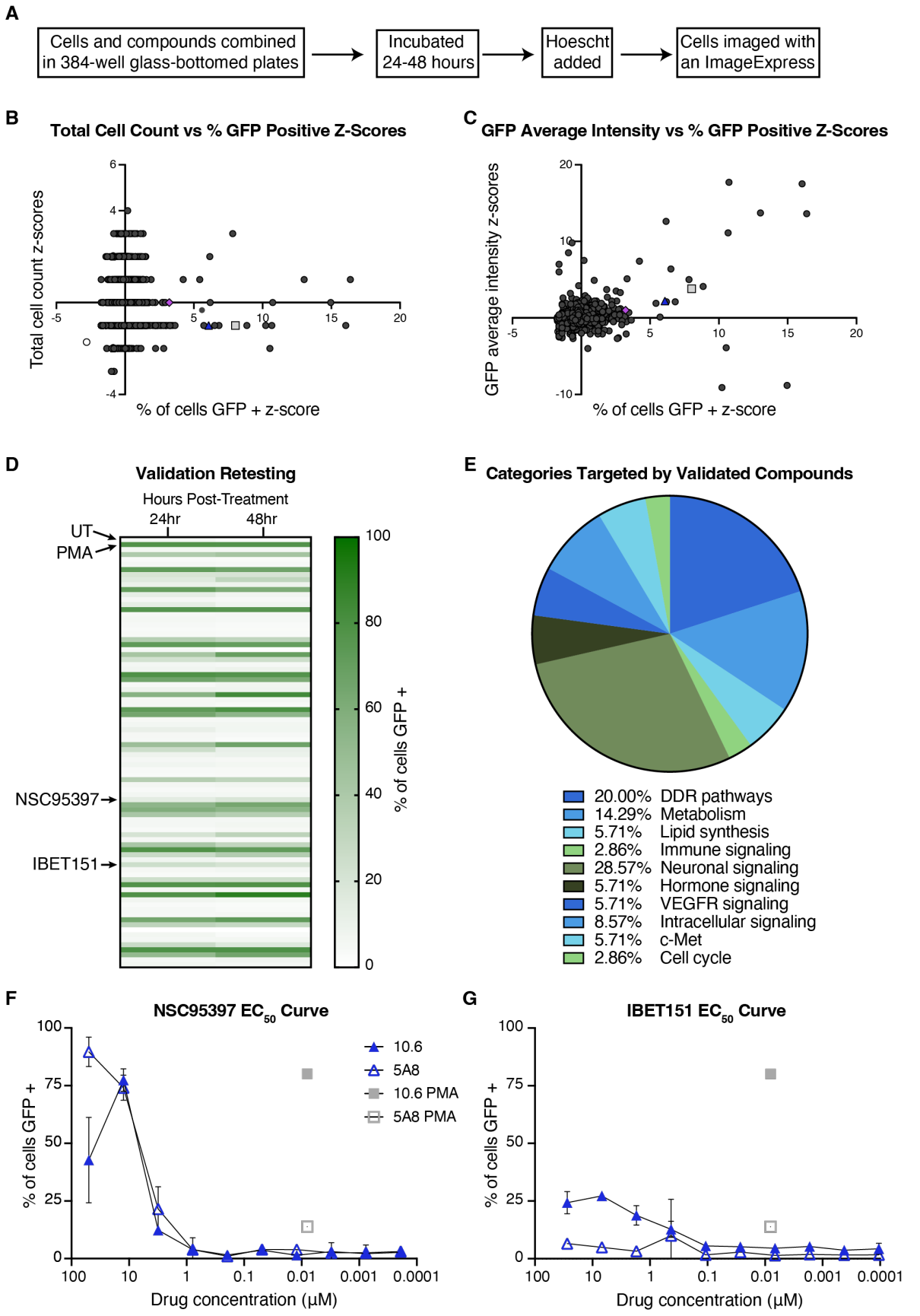
A
Cells and compounds combined in 384-well glass-bottomed plates
Incubated 24-48 hours
Hoescht added
Cells imaged with an ImageExpress
B
Total Cell Count vs % GFP Positive Z-Scores
Total cell count z-scores
% of cells GFP + z-score
C
GFP Average Intensity vs % GFP Positive Z-Scores
GFP average intensity z-scores
% of cells GFP + z-score
D
Validation Retesting
Hours Post-Treatment
24hr
48hr
UT
PMA
NSC95397
IBET151
% of cells GFP +
E
Categories Targeted by Validated Compounds
20.00% DDR pathways
14.29% Metabolism
5.71% Lipid synthesis
2.86% Immune signaling
28.57% Neuronal signaling
5.71% Hormone signaling
5.71% VEGFR signaling
8.57% Intracellular signaling
5.71% c-Met
2.86% Cell cycle
F
NSC95397 EC50 Curve
10.6
5A8
10.6 PMA
5A8 PMA
% of cells GFP +
Drug concentration (μM)
G
IBET151 EC50 Curve
% of cells GFP +
Drug concentration (μM)

631 **Figure 1. NSC95397 identified as a HIV latency reversal agent (LRA) from a medium-**
632 **throughput screen. A)** Schematic detailing the screen methodology. **B-C)** Z-scores of total cell
633 count or GFP intensity vs percent of cells GFP positive. The grey square and purple diamond are
634 two known latency reversal agents, PMA and IBET151, respectively, and the blue triangle is a
635 previously unknown LRA, NSC95397. **D)** 83 compounds were rescreened in triplicate at 24 and
636 48 hours. Each row of the heatmap represents a different compound, with the top and second
637 row being the controls: untreated (UT) and PMA. **E)** A circle graph representing the
638 pathways/targets of the 35 compounds that revalidated in **D**. **F-G)** The EC_{50} titration of NSC95397
639 and IBET151 in J-Lat 10.6 and 5A8 cells. PMA was used as a positive control at 50 nM.

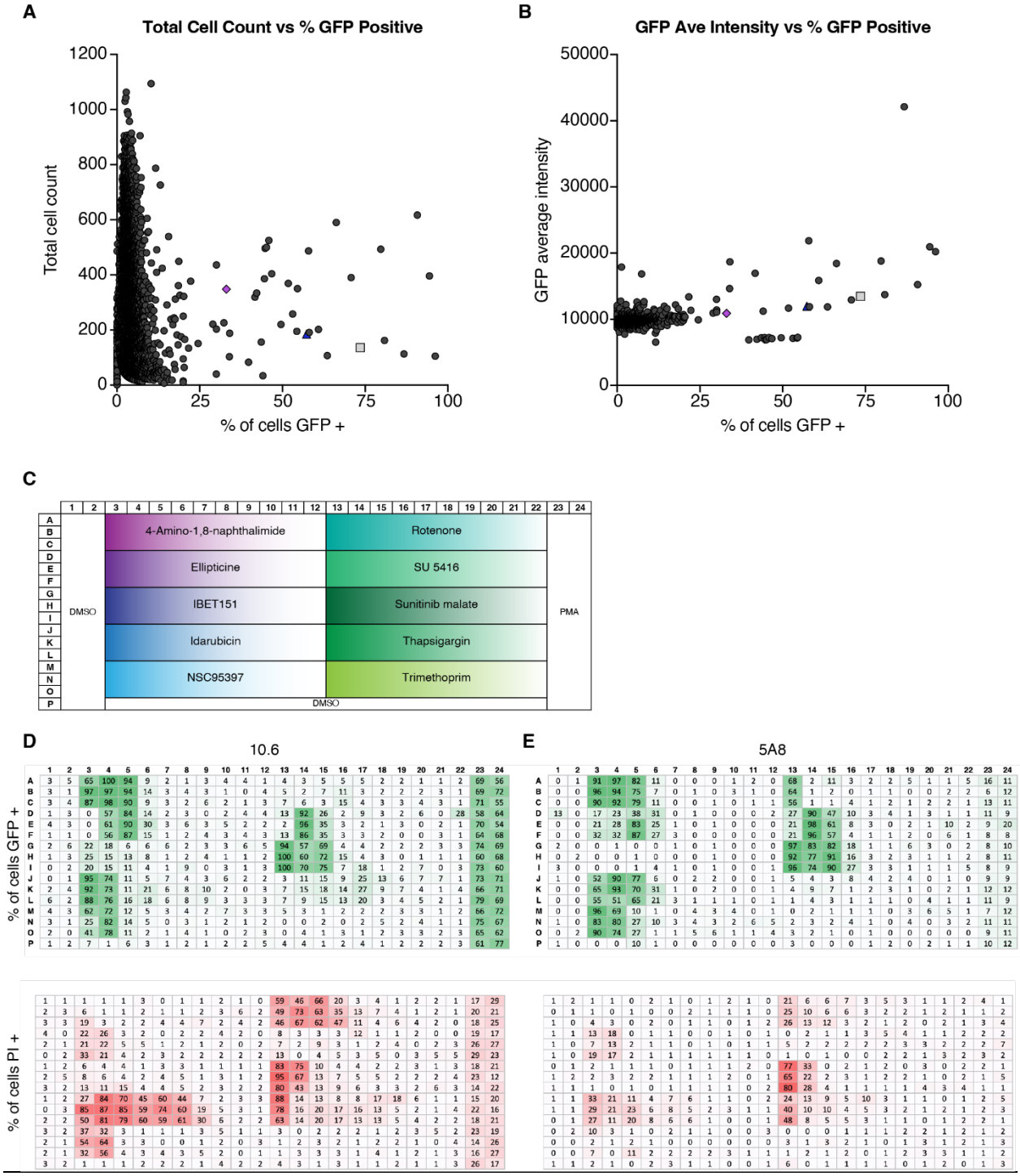

Supplemental Figure 1. NSC95397 and IBET151 were identified as HIV LRAs of interest from a medium-throughput screen. A-B) The raw screen data of total cell count or GFP intensity vs percent of cells GFP positive. The grey square and purple diamond are two known latency reversal agents, PMA and IBET151, respectively, and the blue triangle is a previously unknown LRA, NSC95397. **C)** Example plate map of the EC_{50} screen. Each compound was screened in triplicate and across the plate is a 4-fold concentration decrease. The first two

648 columns and last row were treated with the vehicle control, DMSO, and the last two columns were
649 treated with the positive control, PMA. **D-E)** The percent of GFP positive cells, top green plate,
650 and dead PI positive cell, lower red plate, measured during our EC50 titration experiment in J-Lat
651 10.6 (**D**) and 5A8 cells (**E**). Related to Figure 1.

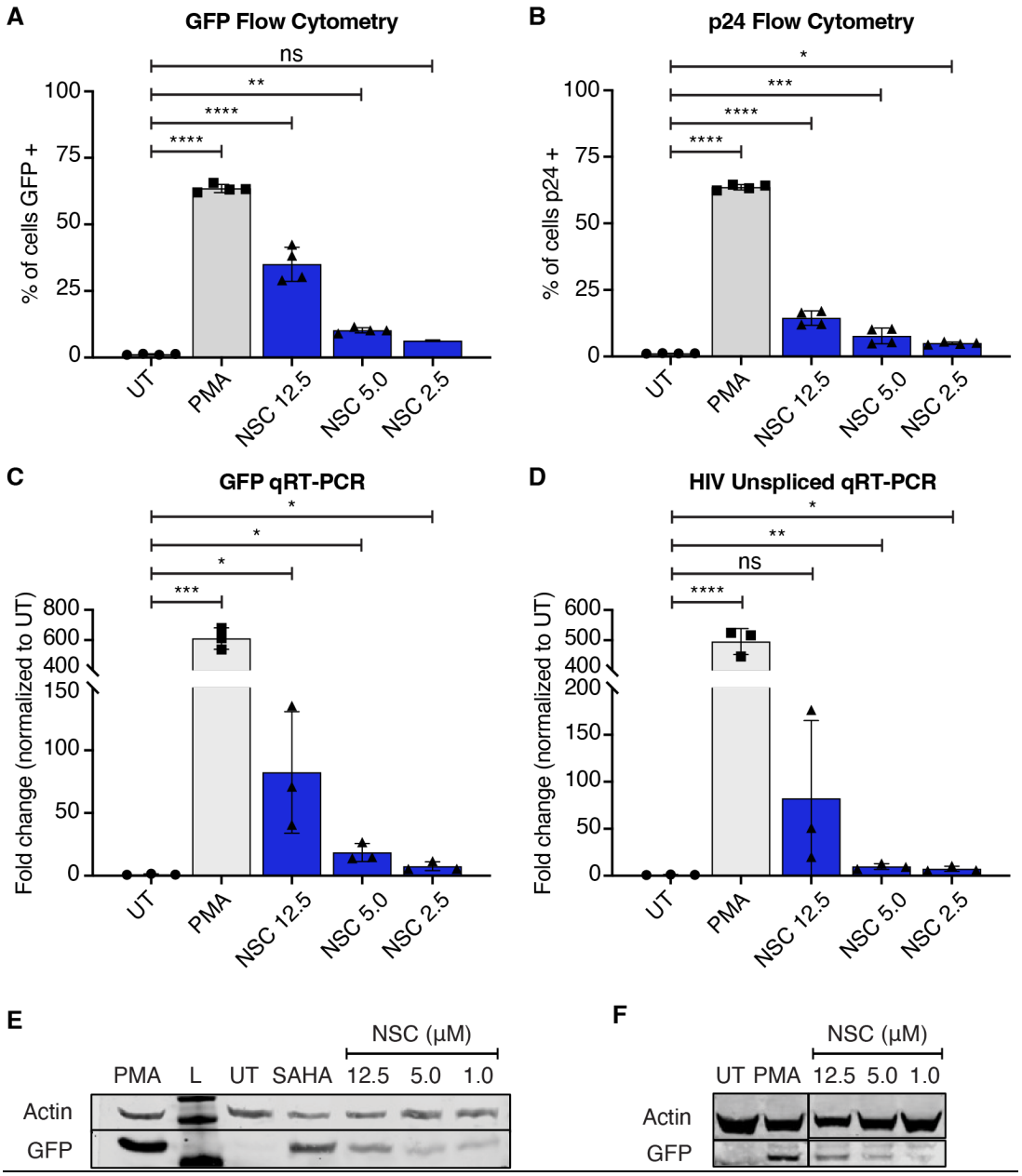

Figure 2. NSC reactivates GFP and p24 expression in J-Lat 10.6 and 5A8 cells. J-Lat 10.6 (**A-E**) or 5A8 (**F**) cells were untreated or treated with 5.0 ng/mL PMA (positive control), or a titration of NSC95397 (NSC) from 12.5 μM to 1.0 μM. **A-B)** Bar graphs showing GFP expression (**A**) or intracellular HIV p24 (**B**) measured via flow cytometry. **C-D)** Bar graphs showing GFP (**C**) or unspliced HIV RNA transcripts (**D**) measured via qRT-PCR. **E-F)** Western blot of whole cell lysates of either J-Lat 10.6 (**E**) or 5A8 cells (**F**) probed for GFP and actin (loading control). 25.0 μM SAHA was used as appositive control. L = ladder; UT = untreated. Results were analyzed with a one-way ANOVA with Dunnett multiple comparisons tests in **A-B** or an unpaired t test in **C-D**; ns = not significant, * = $p \leq 0.0332$, ** = $p \leq 0.0021$, *** = $p \leq 0.0002$, **** = $p \leq 0.0001$.

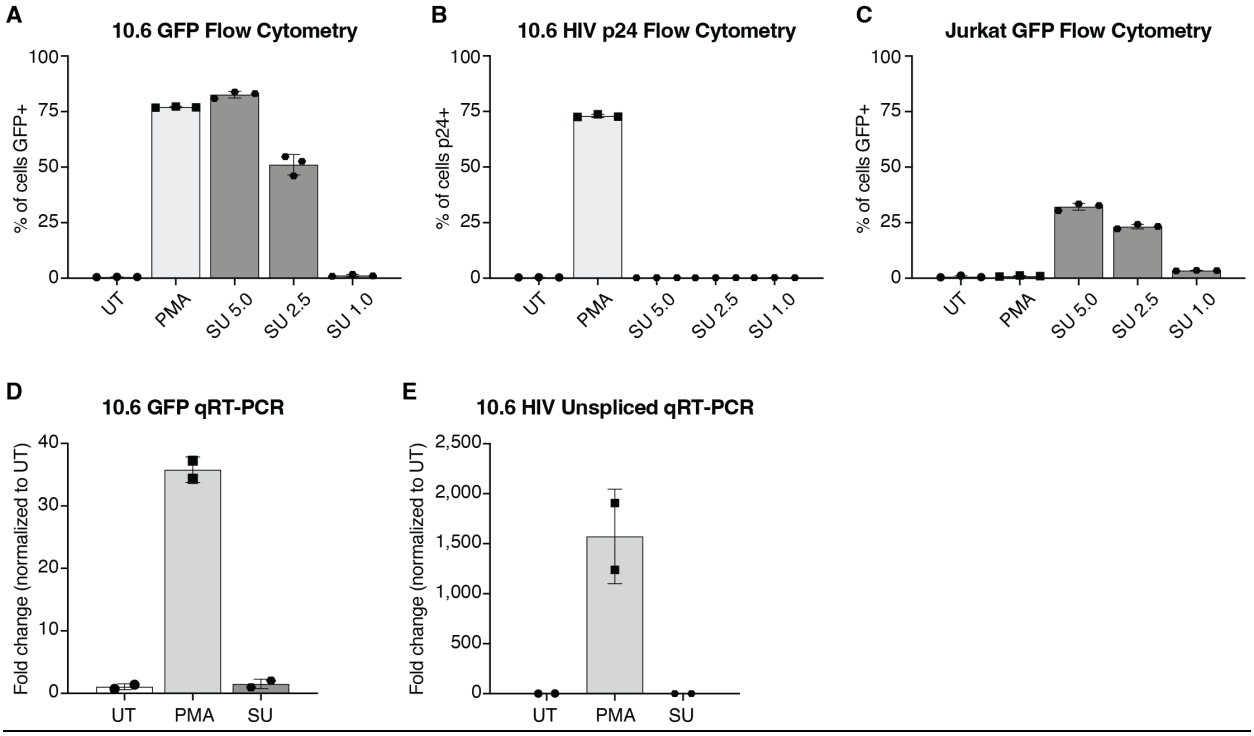

Supplemental Figure 2. Sunitinib is one of a subset of false positives identified in a J-Lat screen for LRAs. J-Lat 10.6 or parental Jurkat cells were untreated or treated with 5.0 ng/mL PMA (positive control), or a titration of Sunitinib (SU) from 5.0 – 1.0 µM. **A-B)** Bar graphs showing GFP (**A**) or intracellular HIV p24 (**B**) measured via flow cytometry in J-Lat 10.6 cells. **C)** A bar graph of GFP measured via flow cytometry in treated Jurkat cells. **D-E)** Bar graphs showing GFP (**D**) or unspliced HIV RNA transcripts (**E**) measured via qRT-PCR. Related to Figure 2.

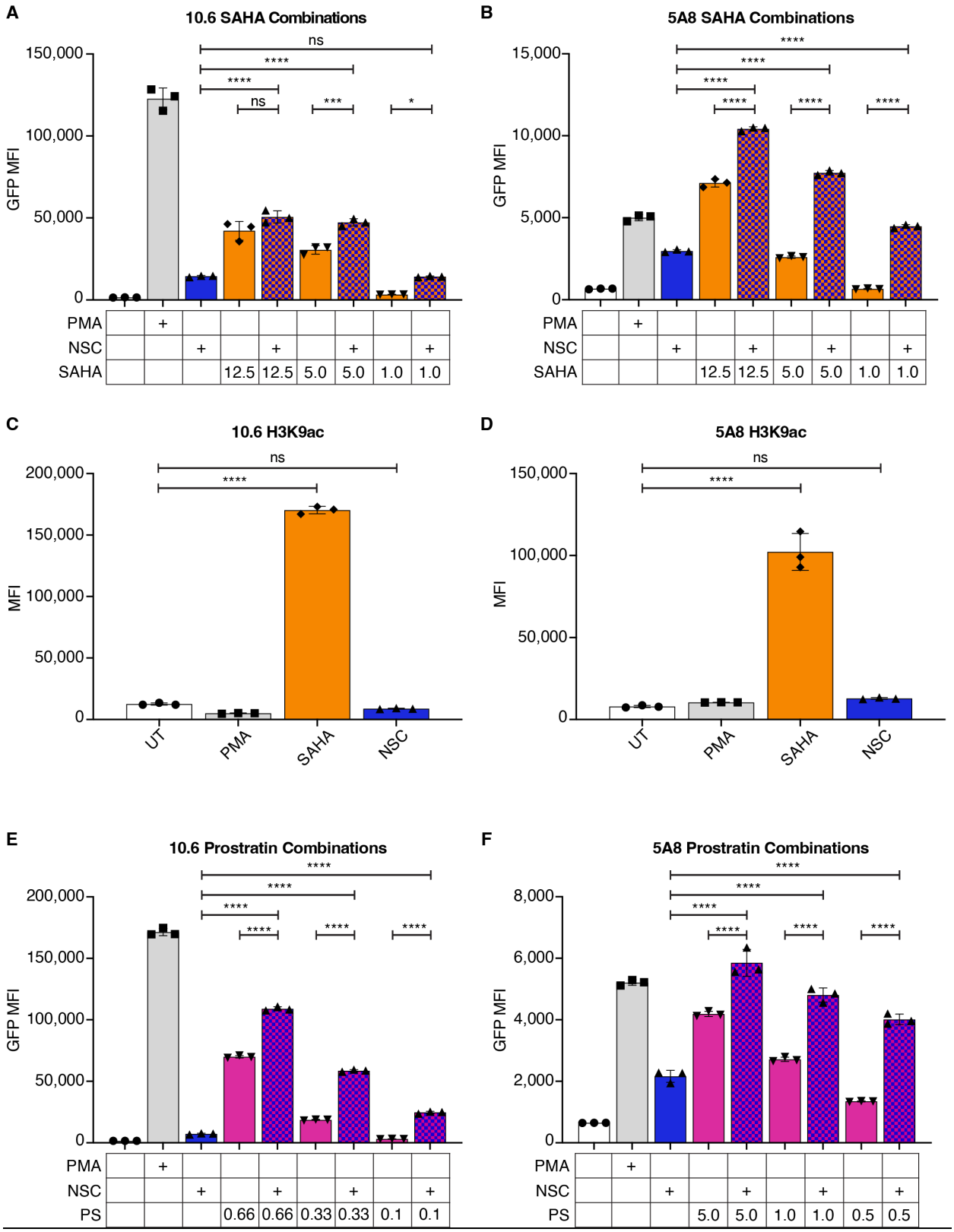

Figure 3. NSC95397 increases HIV reactivation in combination with established LRAs. A-B) J-Lat 10.6 (**A**) or 5A8 (**B**) cells were untreated or treated with 5.0 ng/mL PMA (positive control),

675 NSC95397 (NSC) at 1.5 µM, a titration of SAHA from 12.5 – 1.0 µM, or a titration of SAHA with
676 NSC held constant at 1.5 µM. Bar graphs show GFP mean fluorescence intensity (MFI) measured
677 via flow cytometry. **C-D)** J-Lat 10.6 (**C**) or 5A8 (**D**) cells were untreated or treated with 5.0 ng/mL
678 PMA, 25.0 µM SAHA (positive control), or NSC at 2.5 µM. Bar graphs show H3K9ac MFI
679 measured by flow cytometry. **E-F)** J-Lat 10.6 (**E**) or 5A8 (**F**) cells were untreated or treated with
680 5.0 ng/mL PMA, NSC at 1.5µM, a titration of Prostratin (PS) from 0.66 – 0.1 µM (**E**) or 5 – 0.5 µM
681 (**F**), or a titration of PS with NSC held constant at 1.5 µM. Bar graphs show GFP MFI measured
682 via flow cytometry. Results were analyzed with a one-way ANOVA with Dunnett multiple
683 comparisons tests; ns = not significant, * = $p \leq 0.0332$, ** = $p \leq 0.0021$, *** = $p \leq 0.0002$, **** =
684 $p \leq 0.0001$.

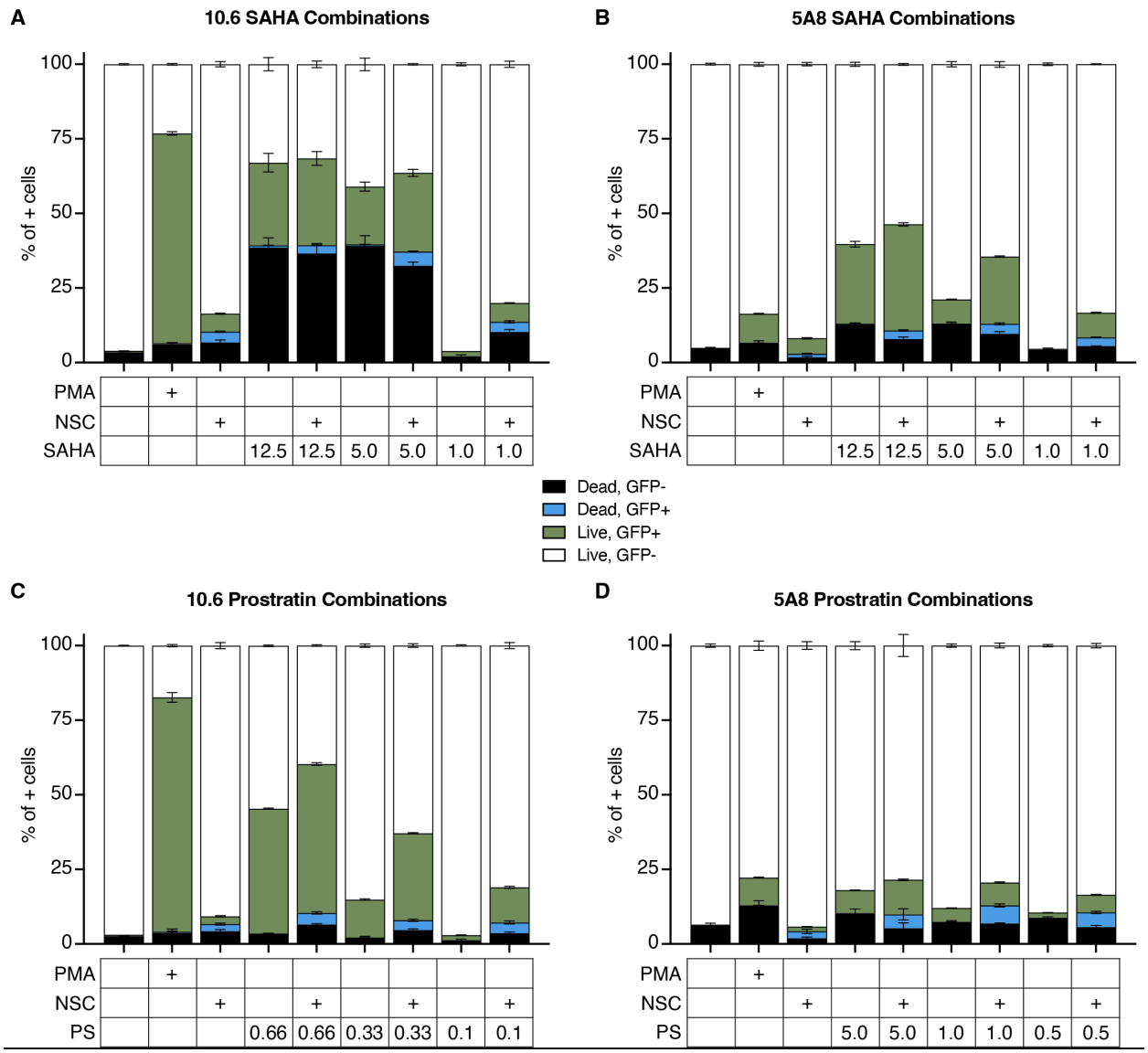

Supplemental Figure 3. NSC95397 increases HIV reactivation and cytotoxicity in combination with established LRAs. Stacked graphs show percent of cells from the full population that are either dead (ghost dye positive) and GFP- (black), dead and GFP+ (blue), live and GFP+ (green), or live and GFP- (white) stacked to a total of 100%. **A-B)** J-Lat 10.6 (**A**) or 5A8 (**B**) cells were untreated or treated with 5.0 ng/mL PMA (positive control), NSC95397 (NSC) at 1.5 µM, a titration of SAHA from 12.5 – 1.0 µM, or a titration of SAHA with NSC held constant at 1.5 µM. **C-D)** J-Lat 10.6 (**C**) or 5A8 (**D**) cells were untreated or treated with 5.0 ng/mL PMA, NSC at 1.5 µM, a titration of Prostratin (PS) from 0.66 – 0.1 µM (**C**) or 5.0 – 0.5 µM (**D**), or a titration of PS with NSC held constant at 1.5 µM. Related to Figure 3 and Supplemental Figure 4.

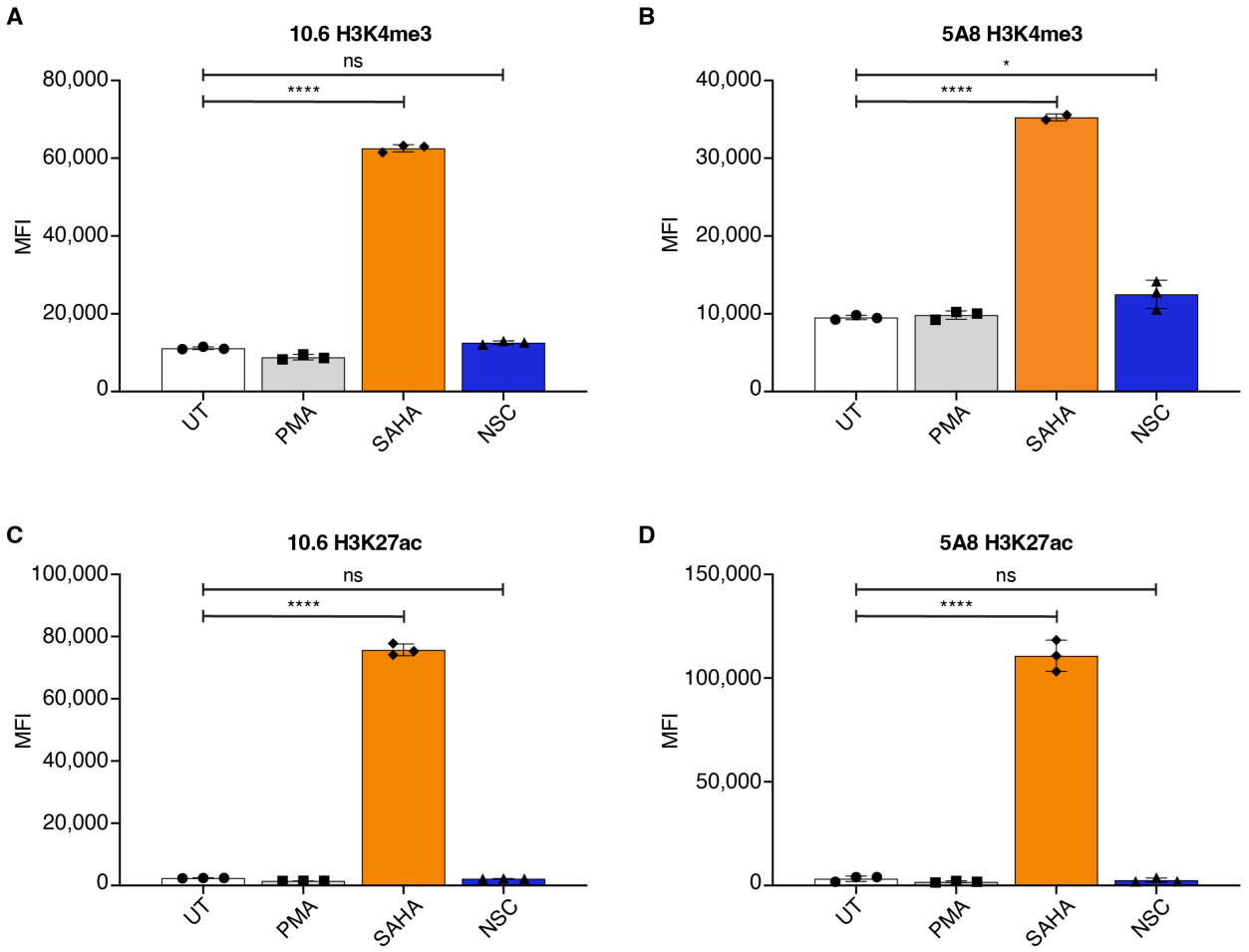

Supplemental Figure 4. NSC95397 does not change global histone modifications for open chromatin. J-Lat 10.6 (**A, C**) or 5A8 (**B, E**) cells were untreated or treated with 5.0 ng/mL PMA, 25.0 µM SAHA (positive control for histone modifications), or 2.5 µM NSC. Bar graphs show H3K4me3 (**A-B**) or H3K27ac (**C-D**) MFI measured by flow cytometry. Results were analyzed with a one-way ANOVA with Dunnett multiple comparisons tests; ns = not significant, * = $p \leq 0.0332$, ** = $p \leq 0.0021$, *** = $p \leq 0.0002$, **** = $p \leq 0.0001$. Related to Figure 3 and Supplemental Figure 3.

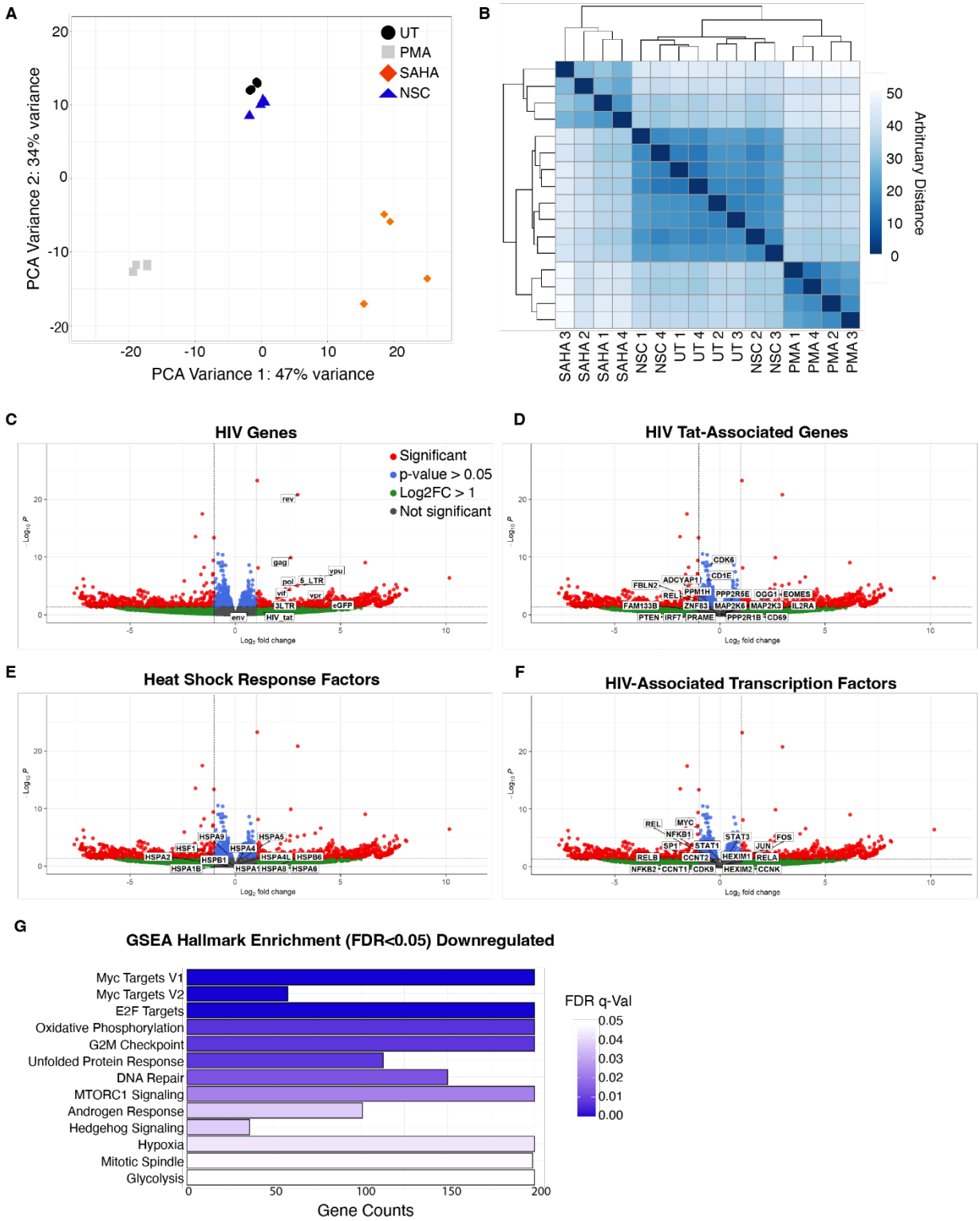

Figure 4. NSC95397 does not globally activate HIV latency reversal associated pathways. J-Lat 10.6 cells were untreated or treated with 5.0 ng/mL PMA, 25.0 µM SAHA, or 5.0 µM SAHA NSC95397 (NSC) and analyzed by bulk RNA sequencing in four biological replicates. **A)** Principal

710 component analysis (PCA) of all normalized transcripts in all samples. **B)** Clustered heatmap of
711 all normalized transcripts in all samples. **C-F)** Volcano plot labeling HIV-associated reads (**C**),
712 selected HIV Tat-modulated genes (**D**), key heat shock response genes (**E**), and HIV-associated
713 transcription factors (**F**). Cut-offs are drawn for log2 fold change above 1 and p-value greater than
714 0.05 where reads are separated to non-significant and non-enriched (gray), non-significant with
715 log2 fold change above 1.0 (green), significant and log2 fold change below 1.0 (blue), or
716 significant and log2 fold change above 1.0 (red). **G)** Gene ontology using Gene Set Enrichment
717 Analysis (GSEA) identifying top negatively enriched hallmarks.

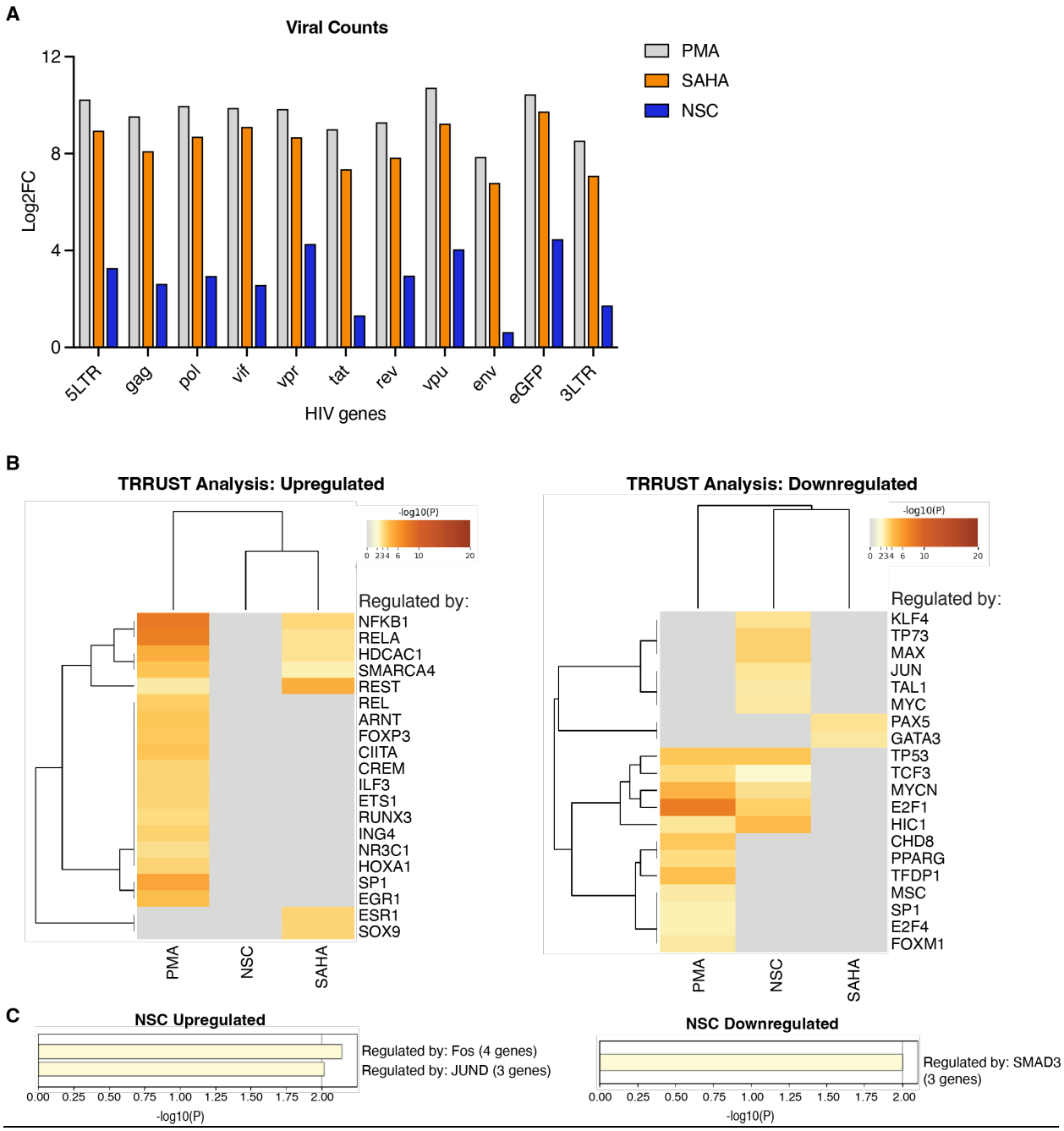

Supplemental Figure 5. NSC95397 has a minimal effect on global transcription. J-Lat 10.6 cells were untreated or treated with 5.0 ng/mL PMA, 25.0 µM SAHA, or 5.0 µM NSC95397 (NSC) and used for bulk RNA sequencing in four biological replicates. **A)** Bar graph showing log2 fold change of HIV associated reads normalizing cells treated with PMA (grey), SAHA (orange), or NSC95397 (blue) against untreated cells. **B-C)** Gene ontology using Metascape for TRRUST analysis of upregulated (left) and downregulated (right) genes for all three treatments (**B**) and NSC95397 alone (**C**). Related to Figure 4 and Supplemental Figure 6.

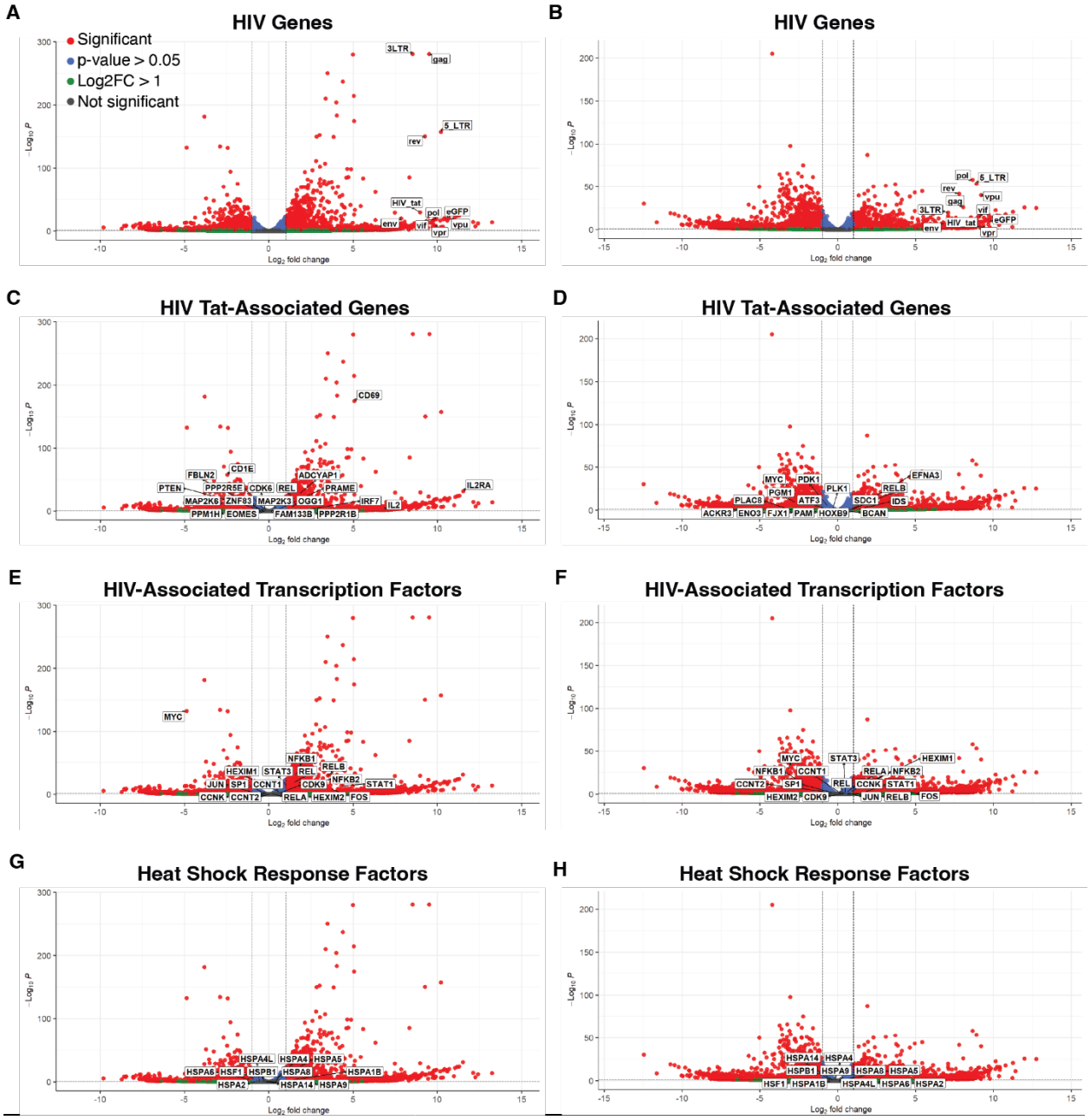

Supplemental Figure 6. PMA and SAHA change latency modulating pathways. J-Lat 10.6 cells were untreated or treated with 5.0 ng/mL PMA or 25.0 µM SAHA and used for bulk RNA sequencing in four biological replicates. **A-B)** Volcano plot highlighting HIV-associated reads in cells treated with PMA (**A**) or SAHA (**B**). **C-D)** Volcano plots highlighting HIV-associated transcription factors in cells treated with PMA (**C**) or SAHA (**D**). **E-F)** Volcano plots highlighting selected HIV Tat-modulated genes in cells treated with PMA (**E**) or SAHA (**F**). **G-H)** Volcano plots highlighting key heat shock response genes in cells treated with PMA (**G**) or SAHA (**H**). Cut-offs are drawn for log2 fold change above 1 and p-value greater than 0.05 where reads are separated to non-significant and non-enriched (gray), non-significant with log2 fold change above 1.0 (green), significant and log2 fold change below 1.0 (blue), or significant and log2 fold change above 1.0 (red). Related to Figure 3 and Supplemental Figure 5.

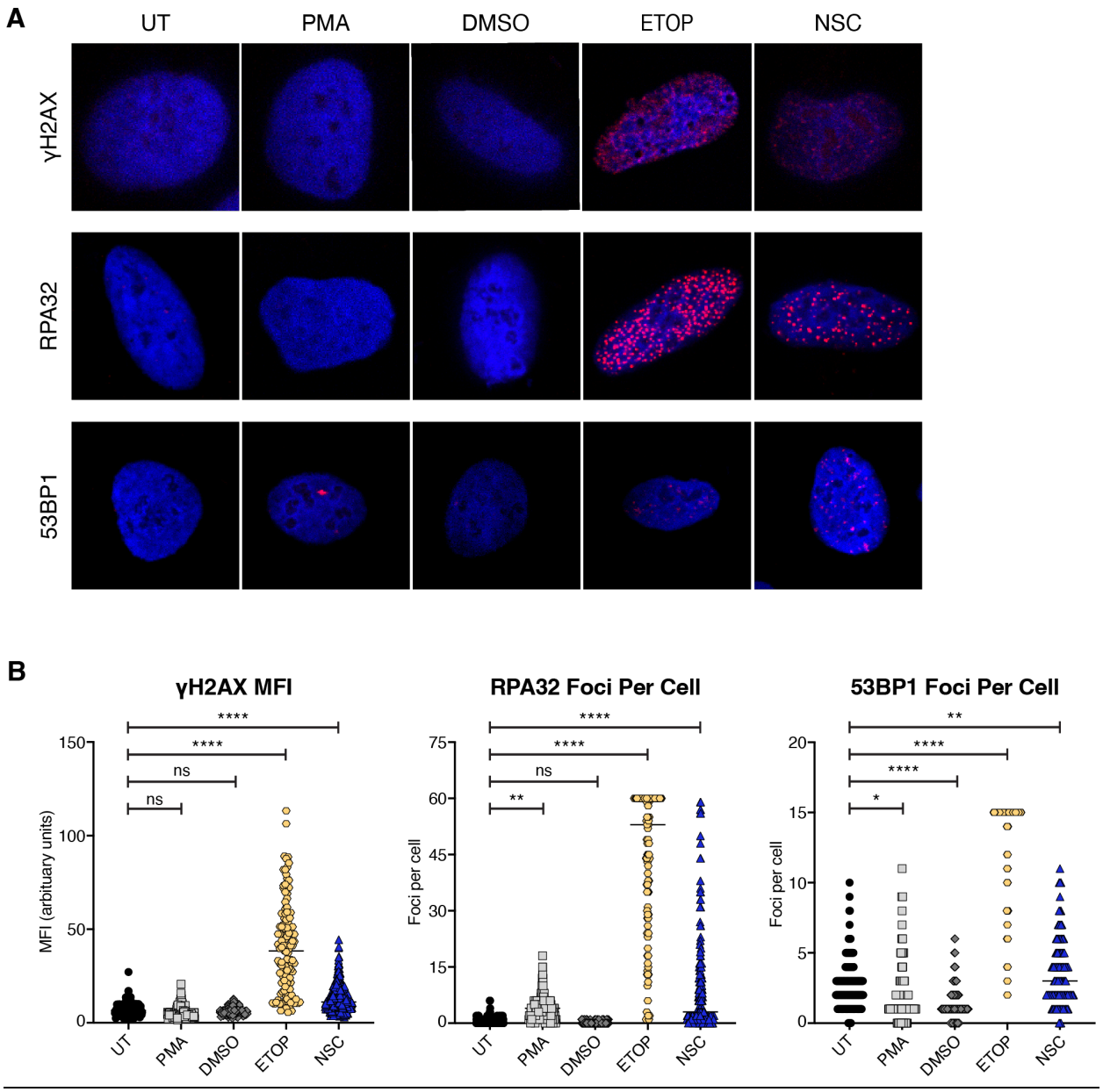

Figure 5. NSC95397 causes accumulation of DNA damage markers. A) Representative images of U2OS cells untreated or treated with 10.0 µL DMSO (negative control), 50.0 µM Etoposide (ETOP; DNA damage positive control), 5.0 ng/mL PMA, or 5.0 µM NSC95397 (NSC) for 24 hours and assessed for presence of DNA damage markers by confocal microscopy. Blue (Hoechst 33342) shows nuclei while damage markers (γH2AX, RPA32, or p53BP1) are in red. **B)** Mean fluorescence intensity (MFI) of at least 100 cells per condition was quantified for γH2AX. Foci per cell of at least 100 cells per condition was quantified for RPA32 and 53BP1 where foci above the ETOP control are binned at 60 (RPA32) or 15 (53BP1). Results were analyzed with a one-way ANOVA with Dunnett multiple comparisons tests; ns = not significant, * = $p \leq 0.0332$, ** = $p \leq 0.0021$, *** = $p \leq 0.0002$, **** = $p \leq 0.0001$.